Supplementary Information

Quantifying Coordination Effects for Rational Design of MXene-Based NRR Electrocatalysts

Shuaipeng Mao[1], Dongyue Gao[1,*], Chen Yang[1], Junxia Li[1], Yi Fang[1], Yang Huang[1], Chengchun Tang[1], Zhonglu Guo[1,*]

[1]*Hebei Key Laboratory of Boron Nitride Micro and Nano Materials*, *School of Materials Science and Engineering, Hebei University of Technology, Tianjin 300130, China*

*Correspondence and requests for materials should be addressed to D. Y. Gao or Z. L. Guo: gaodongyue9@163.com, zlguo@hebut.edu.cn.

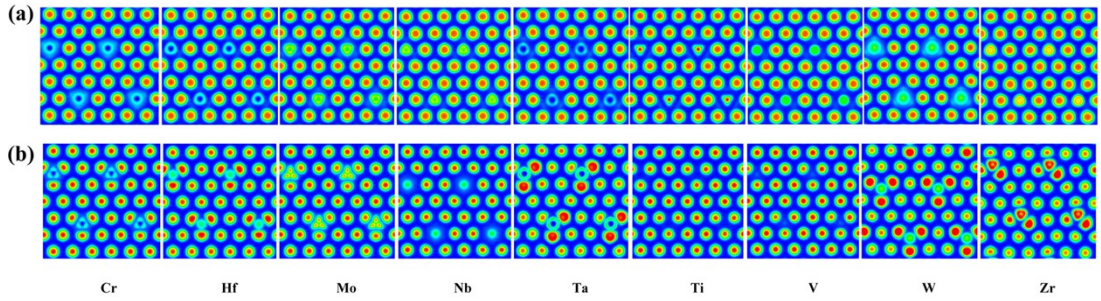

Fig. S1. Electron localization function (ELF) plots of $Mo_2TiC_2O_2$ under (a) doped and (b) anchored

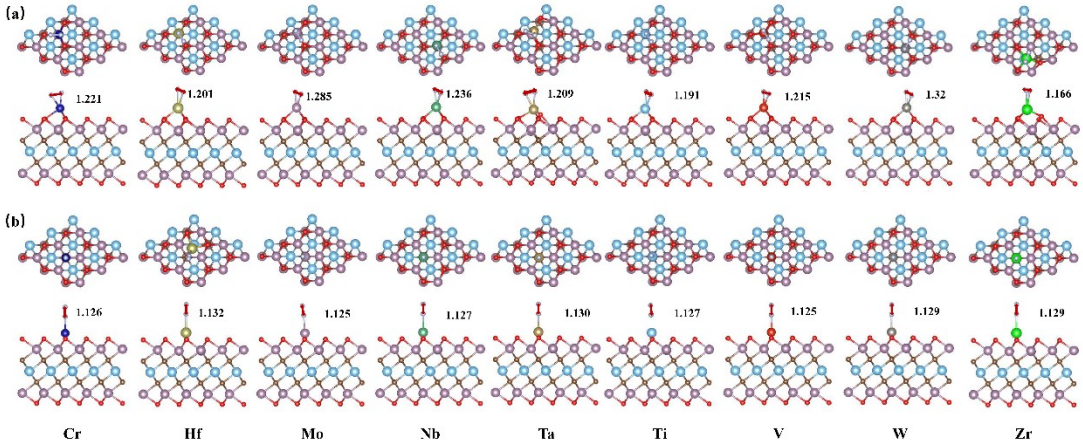

Fig. S2. Optimized structures of N_2 adsorbed at anchored and doped configurations on $Mo_2TiC_2O_2$ through (a) side-on on anchored and (b) end-on on doped. N-N bond lengths are given.

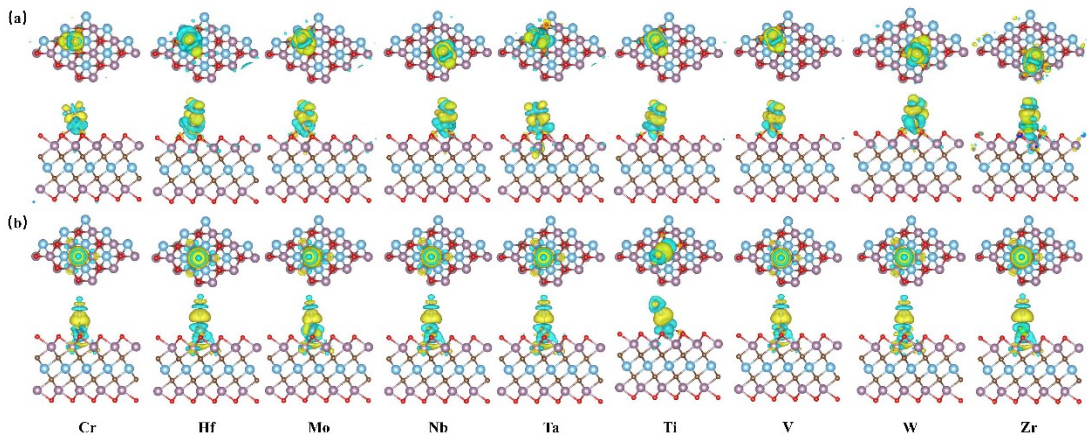

Fig. S3. Charge density differences of N_2 adsorbed on $Mo_2TiC_2O_2$ with different configurations by the (a) side-on and (b) end-on patterns. The isosurface value is 0.001 $e \cdot Å^{-3}$.

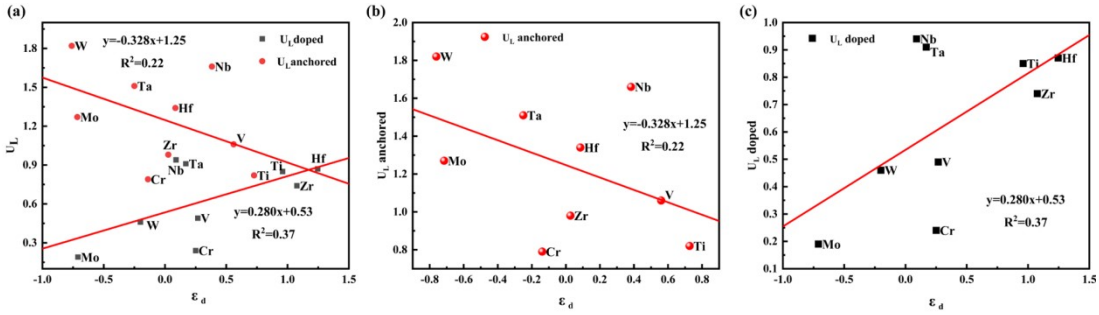

Fig. S4. ε_d of transition metals versus U_L

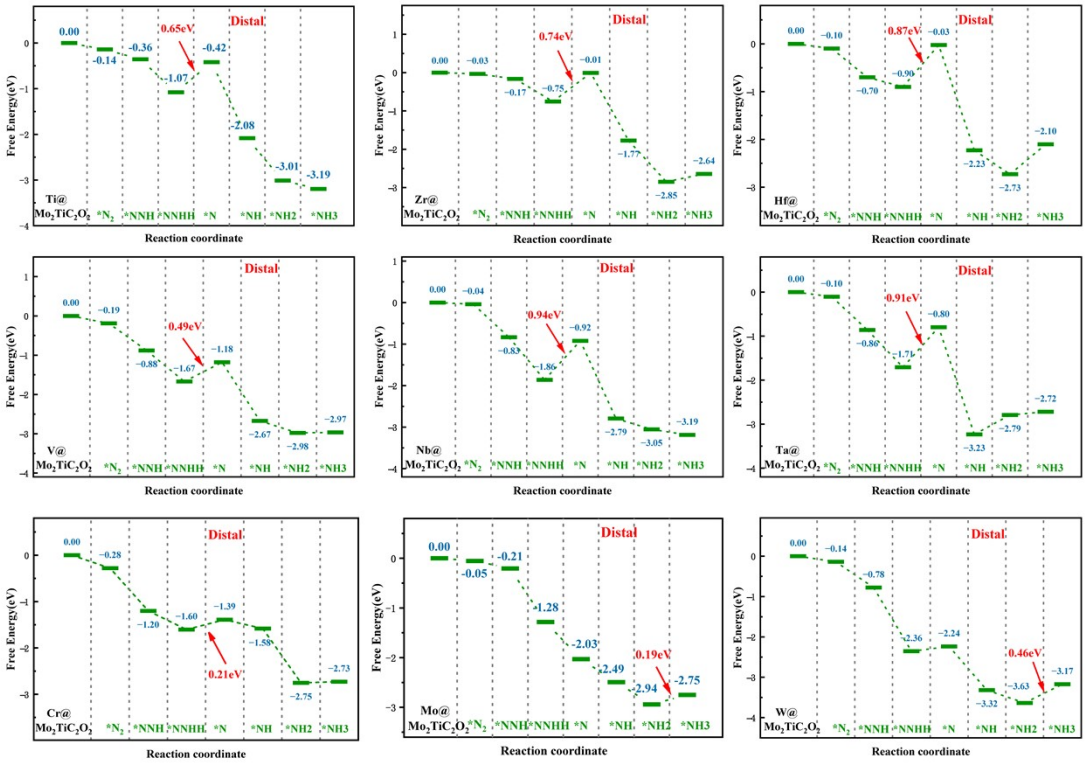

Fig. S5. Gibbs free energy diagrams for N_2 electroreduction through the distal pathway on metal doped $Mo_2TiC_2O_2$

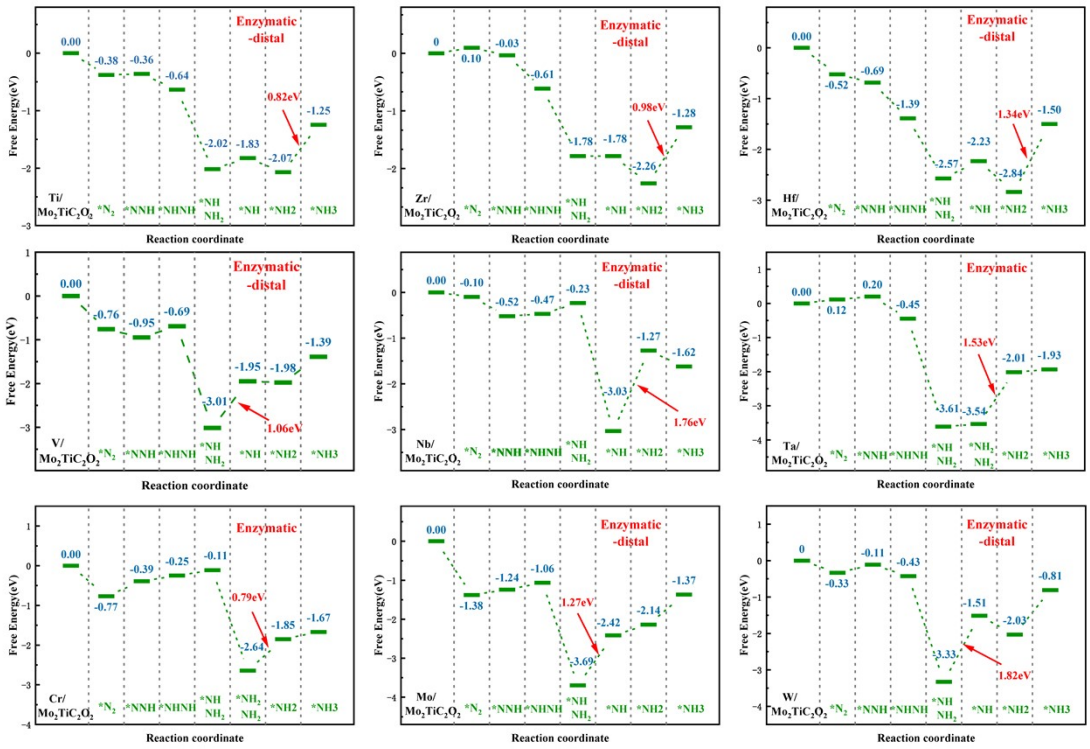

Fig. S6. Gibbs free energy diagrams for N_2 electroreduction through the enzymatic and enzymatic-distal pathways on metal anchored $Mo_2TiC_2O_2$

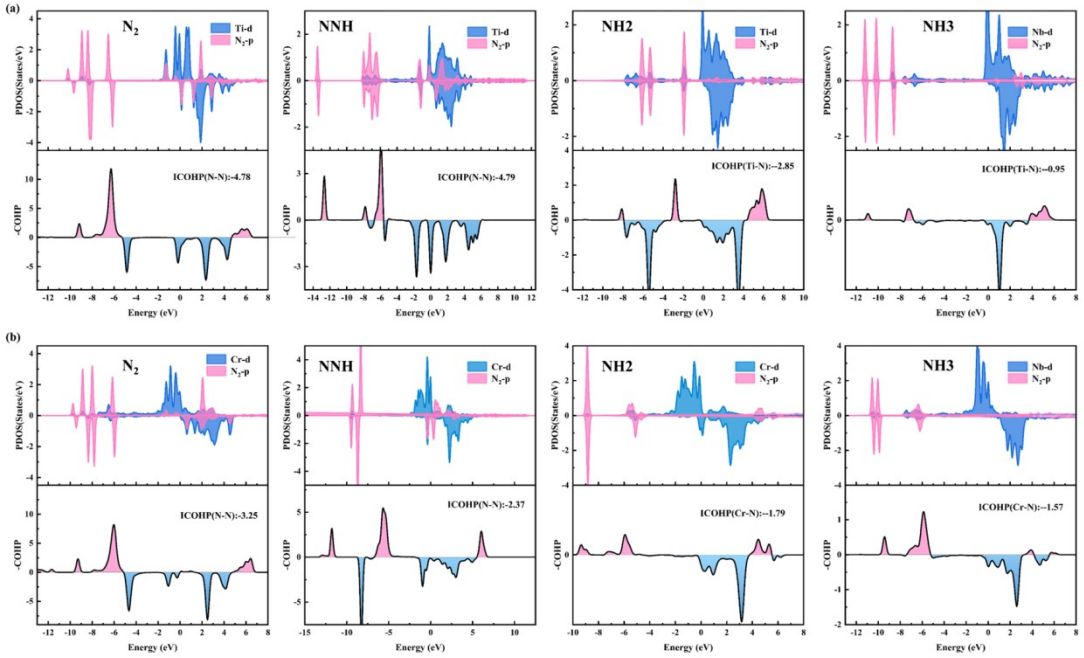

Fig S7. PDOS and the COHP patterns for the four key intermediates N_2*, NNH*, NH_2* and NH_3*on (a)Ti/$Mo_2TiC_2O_2$ and (b) Cr/$Mo_2TiC_2O_2$

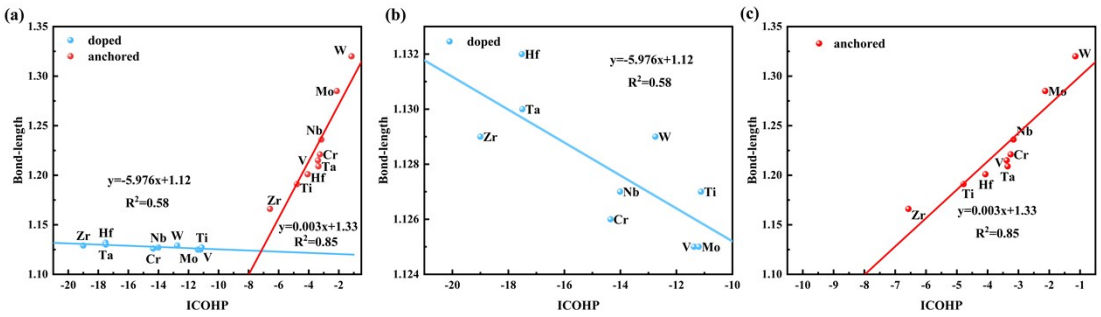

Fig S8. Linear relationship for bond length versus COHP values between N and N atoms of doped and anchored system on $Mo_2TiC_2O_2$

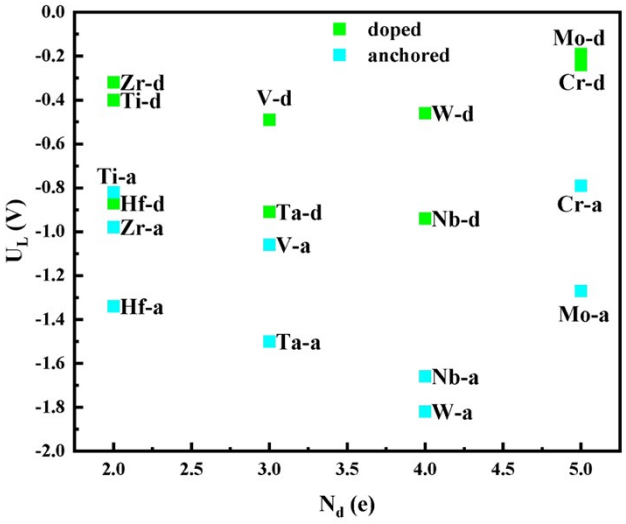

Fig S9. Relationship between U_L versus N_d (the sum of the number of d orbital electron of bimetal).

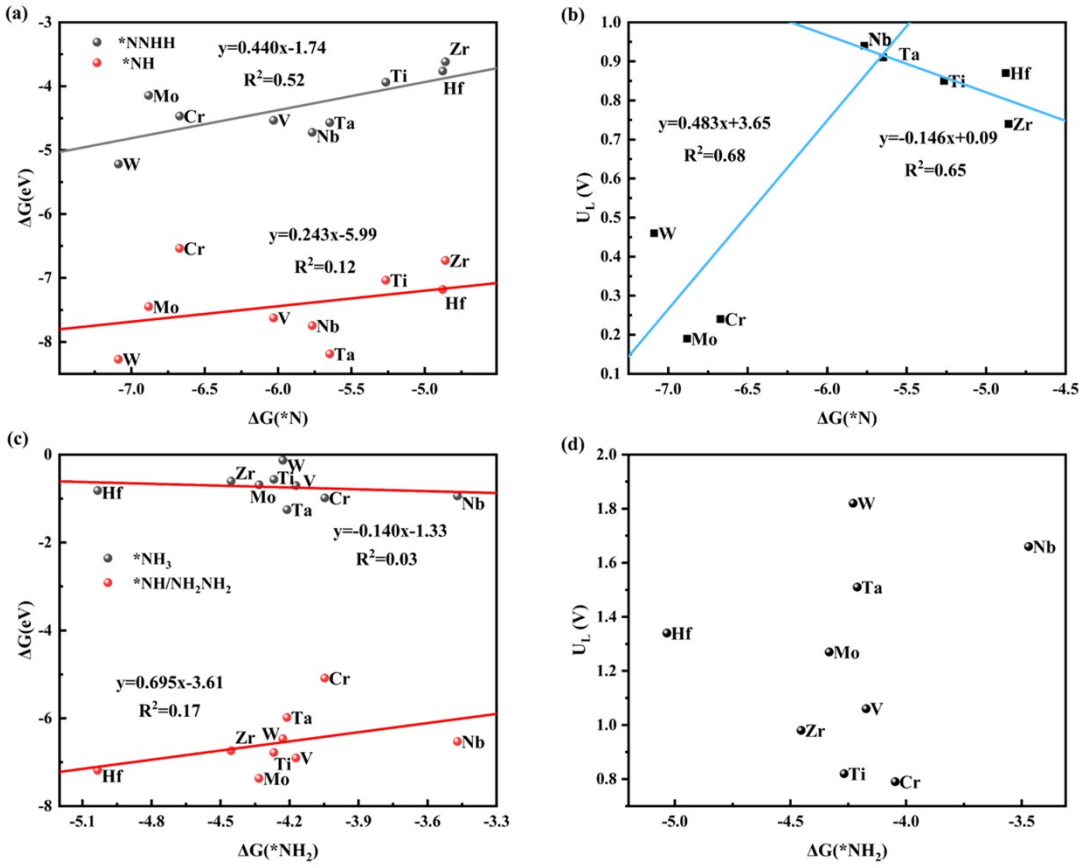

Fig S10. (a) Adsorption free energy relationship of ΔG(NNHH*) and ΔG(NH*) versus ΔG(N*). (b) The NRR volcano plot of metal doped $Mo_2TiC_2O_2$ in which ΔG(N*) acts as the descriptor of U_L. (c) Adsorption free energy relationship of ΔG(NH_3*) and ΔG(NH/NH_2NH_2*) versus ΔG(NH_2*) (d) The NRR volcano plot of metal anchored $Mo_2TiC_2O_2$ in which ΔG(NH_2*) acts as the descriptor of U_L.

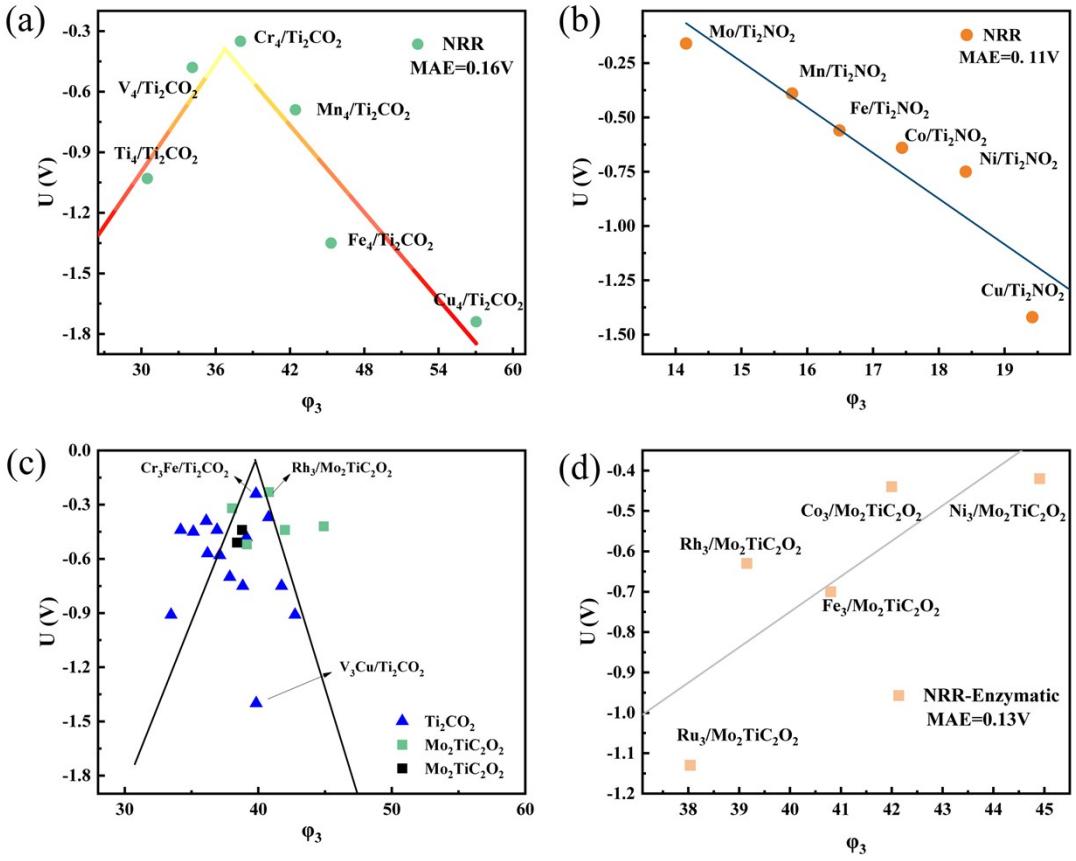

Fig S11. Relationships between the limiting potentials for (a) TM_4/Ti_2CO_2,[3] (b) TM/Ti_2NO_2[2], (c) M_2M'/Ti_2CO_2, $M_3/Mo_2TiC_2O_2$[4] and (d) M_3M'/Ti_2CO_2[3] of MXene-supported single atom, homonuclear cluster, heteronuclear cluster, and the descriptor φ_3.

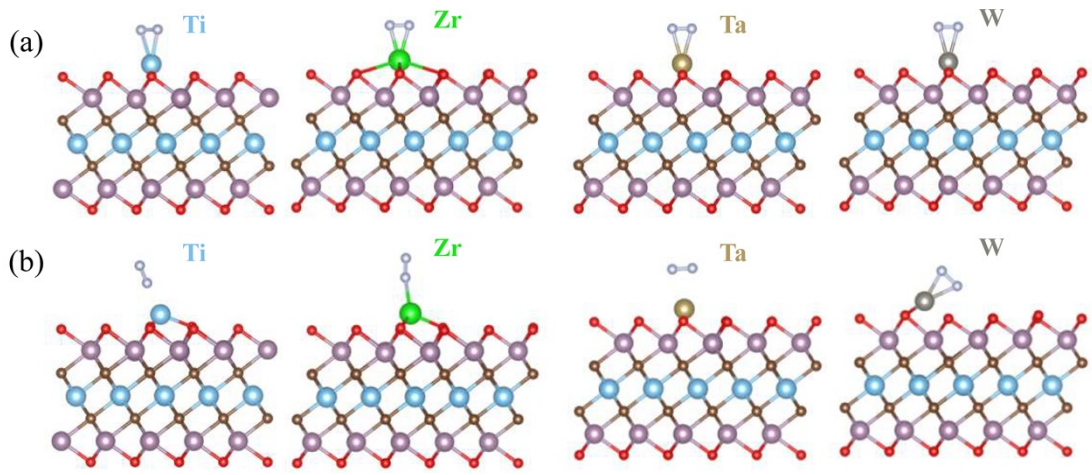

Fig S12. Comparison of the initial side-on adsorption configurations and the optimized structures for N_2 adsorption on Ti-, Zr-, Ta-, and W-doped $Mo_2TiC_2O_2$ (a) initial side-on adsorption geometries before structural optimization (b) optimized adsorption geometries after structural relaxation.

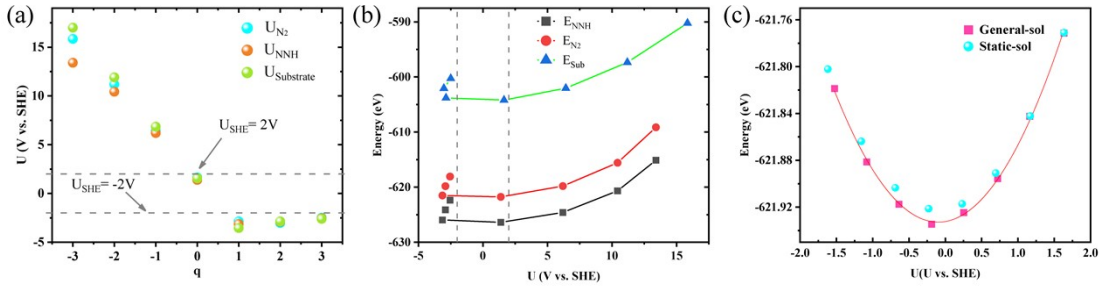

Fig S13. (a) Relationship between the applied excess charge and the effective electrode potential within the constant-charge implicit solvent model. The light gray dashed lines indicate the potential window of −2.0 to 2.0 V (b) Potential-dependent energy variations of representative reaction intermediates, illustrating the systematic response of adsorption energetics to the applied electrode potential. The light gray dashed lines denote −2.0 and 2.0 V (c) Dependence of reaction free energy of N_2* on potential referenced to the RHE scale (U_{RHE}) in the range from −2.0 to 2.0 V, exhibiting an upward-opening quadratic behavior.

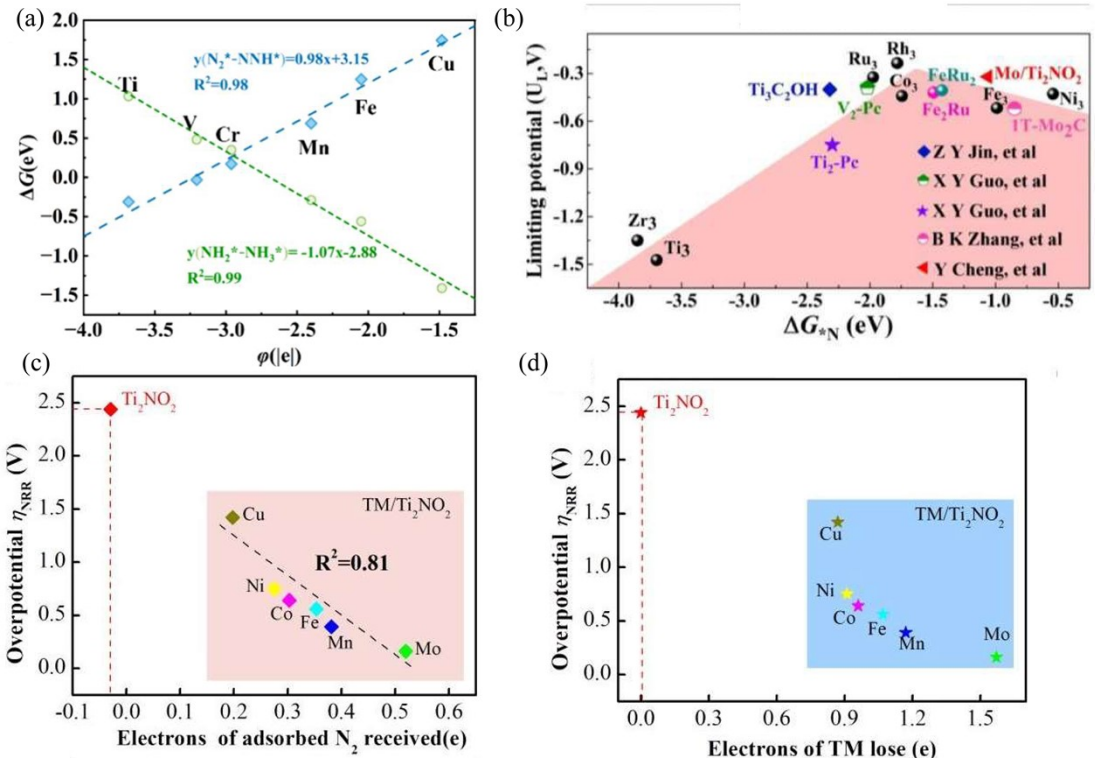

Fig S14. (a) Linear relationships of $\Delta G(N_2{*}{-}NNH{*})$ and $\Delta G(NH_2{*}{-}NH_3{*})$ vs descriptor φ(|e|) of M_4/Ti_2CO_2[3] (b) Volcano curves of limiting potential U_L and *N adsorption free energy (ΔG_{*N}) for M_3 SCCs[4](c) η_{NRR} against the electrons of adsorbed N_2 received, (d) η_{NRR} against the electrons of TM losing[2]

Table S1. Binding energies of doped metals and charge transfer of adsorbed nitrogen on $Mo_2TiC_2O_2$.

System	E_b(eV)	Charge~M-N_2(|e|)
Ti@$Mo_2TiC_2O_2$	-4.90	0.17
V@$Mo_2TiC_2O_2$	-5.42	0.18
Cr@$Mo_2TiC_2O_2$	-4.86	0.15
Zr@$Mo_2TiC_2O_2$	-5.79	0.25
Nb@$Mo_2TiC_2O_2$	-6.86	0.19
Mo@$Mo_2TiC_2O_2$	-7.29	0.16
Hf@$Mo_2TiC_2O_2$	-3.67	0.24
Ta@$Mo_2TiC_2O_2$	-4.70	0.25
W@$Mo_2TiC_2O_2$	-5.32	0.21

Table S2. Binding energies of anchored metals and charge transfer of adsorbed nitrogen on $Mo_2TiC_2O_2$.

System	E_b(eV)	Charge~M-N_2(|e|)
Ti/$Mo_2TiC_2O_2$	-19.69	0.55
V/$Mo_2TiC_2O_2$	-16.28	0.60
Cr/$Mo_2TiC_2O_2$	-14.53	0.51
Zr/$Mo_2TiC_2O_2$	-19.89	0.42
Nb/$Mo_2TiC_2O_2$	-12.43	0.72
Mo/$Mo_2TiC_2O_2$	-12.74	0.70
Hf/$Mo_2TiC_2O_2$	-13.34	0.66
Ta/$Mo_2TiC_2O_2$	-18.15	0.62
W/$Mo_2TiC_2O_2$	-18.81	0.82

Table S3. Adsorption energies for end-on and side-on adsorption configurations on metal-doped $Mo_2TiC_2O_2$ and metal-anchored $Mo_2TiC_2O_2$ systems.

Metal	Adsorption energies (eV)			
	End-on		Side-on	
	Anchored	Doped	Anchored	Doped
Ti	-0.15	-0.14	-0.38	-1.32
V	-0.52	-0.19	-0.76	0.27
Cr	-0.70	-0.28	-0.77	0.22
Zr	-0.04	-0.03	0.10	-1.10
Nb	0.41	-0.04	-0.10	0.40
Mo	-0.81	-0.05	-1.38	-0.78
Hf	-0.35	-0.10	-0.52	-1.51
Ta	0.05	-0.10	0.12	-0.4
W	0.53	-0.14	-0.33	-1.31

For several doped systems, the initially constructed side-on N_2 adsorption relaxes into an end-on geometry during optimization; in such cases, the reported adsorption energies correspond to the fully relaxed final structures, and the initial side-on configuration is not treated as a stable local minimum

Table S4. N-N bond lengths of N_2 adsorption and U_L on metal-doped and metal-anchored $Mo_2TiC_2O_2$ systems.

Metal	Anchored		Doped	
	N-N-length (Å)	U_L (V)	N-N-length (Å)	U_L (V)
Ti	1.191	0.82	1.127	0.85
V	1.215	1.06	1.125	0.49
Cr	1.221	0.79	1.126	0.21
Zr	1.166	0.98	1.129	0.74
Nb	1.236	1.66	1.127	0.94
Mo	1.285	1.27	1.125	0.19
Hf	1.201	1.34	1.132	0.87
Ta	1.209	1.51	1.130	0.91
W	1.320	1.82	1.129	0.46

Table S5. The ΔG of potential-determined step (ΔG(NNHH*-N*) and ΔG(NH_2*-NH_3*)) of 9 doped metals (i.e., Ti@$Mo_2TiC_2O_2$, V@$Mo_2TiC_2O_2$, Cr@$Mo_2TiC_2O_2$, Zr@$Mo_2TiC_2O_2$,Nb@$Mo_2TiC_2O_2$,Mo@$Mo_2TiC_2O_2$,Hf@$Mo_2TiC_2O_2$,Ta@$Mo_2TiC_2O_2$, W@$Mo_2TiC_2O_2$).

	ΔG(NNHH*-N*) (eV)	ΔG(NH_2*-NH_3*) (eV)	ΔG_{max}(eV)
Ti@$Mo_2TiC_2O_2$	0.65	-0.18	0.65
V@$Mo_2TiC_2O_2$	0.49	0.01	0.49
Cr@$Mo_2TiC_2O_2$	0.21	0.02	0.21
Zr@$Mo_2TiC_2O_2$	0.74	0.21	0.74
Nb@$Mo_2TiC_2O_2$	0.94	-0.14	0.94
Mo@$Mo_2TiC_2O_2$	-0.75	0.19	0.19
Hf@$Mo_2TiC_2O_2$	0.87	0.63	0.87
Ta@$Mo_2TiC_2O_2$	0.91	0.07	0.91
W@$Mo_2TiC_2O_2$	0.12	0.46	0.46

Table S6. The ΔG of potential-determined step (ΔG($NHNH_2$*-NH*/NH_2NH_2), ΔG(NH/NH_2NH_2*-NH_2*) and ΔG(NH_2*-NH_3*)) of 9 anchored metals (i.e., Ti/$Mo_2TiC_2O_2$,V/$Mo_2TiC_2O_2$,Cr/$Mo_2TiC_2O_2$,Zr/$Mo_2TiC_2O_2$,Nb/$Mo_2TiC_2O_2$,Mo/$Mo_2TiC_2O_2$,Hf/$Mo_2TiC_2O_2$,Ta/$Mo_2TiC_2O_2$, W/$Mo_2TiC_2O_2$).

Adsorption energies (eV)	ΔG($NHNH_2$*-NH*/NH_2NH_2) (eV)	ΔG(NH/NH_2NH_2*-NH_2*) (eV)	ΔG(NH_2*-NH_3*) (eV)	ΔG_{max}(eV)
Ti/$Mo_2TiC_2O_2$	0.19	-0.24	0.82	0.82
V/$Mo_2TiC_2O_2$	1.06	-0.03	0.59	1.06
Cr/$Mo_2TiC_2O_2$	-2.53	0.79	0.18	0.79
Zr/$Mo_2TiC_2O_2$	0	-0.48	0.98	0.98
Nb/$Mo_2TiC_2O_2$	-2.8	1.76	-0.35	1.76
Mo/$Mo_2TiC_2O_2$	1.27	0.28	0.77	1.27
Hf/$Mo_2TiC_2O_2$	0.34	-0.61	1.34	1.34
Ta/$Mo_2TiC_2O_2$	0.07	1.53	0.08	1.53
W/$Mo_2TiC_2O_2$	1.82	-0.52	1.22	1.82

Table S7. The ΔG (N_2*-NNH*) of metal doped and anchored systems

Metal	Anchored		Doped	
	Side-on	End-on	Side-on	End-on
Cr	0.38	0.23	/	/
Mo	/	/	-0.83	-0.16
Ta	0.08	0.45	/	/
W	/	/	0.34	-0.64

Table **S8.** Detailed information of seven embedded candidates. Elements are arranged in atomic number. [1]

	ΔEN_2-adsorption[eV]	PDS	ΔGmax[eV]	ΔGNH_3-adsorption[eV]
Zr	-0.57	$*N_2 \rightarrow *NNH$	0.15	0.97
Mo	-0.58	$*NH_2 \rightarrow *NH_3$	0.51	0.58
Hf	-0.52	$*NH \rightarrow *NH_2$	0.25	0.98
Ta	-0.31	$*NH \rightarrow *NH_2$	0.21	0.77
W	-0.43	$*NH \rightarrow *NH_2$	0.46	0.81
Re	-0.51	$*NH \rightarrow *NH_2$	0.47	0.81
Os	-0.42	$*NH \rightarrow *NH_2$	0.32	0.72

Table **S9.** The calculated ηNRR and electrons (based Bader charge analysis) of adsorbed N_2 receiving and TM losing of TM/Ti_2NO_2 systems.[2]

Systems	ηNRR (V)	adsorbed N_2 receiving electrons(e)	TM losing electrons (e)
Mo/Ti_2NO_2	0.16	0.52	1.58
Mn/Ti_2NO_2	0.39	0.38	1.17
Fe/Ti_2NO_2	0.56	0.35	1.07
Co/Ti_2NO_2	0.64	0.30	0.96
Ni/Ti_2NO_2	0.75	0.27	0.91
Cu/Ti_2NO_2	1.42	0.19	0.87
Ti_2NO_2	2.44	-0.03	-

Table **S10.** The ΔG of rate-determined step (ΔG(N_2*-NNH*) and ΔG(NH_2*-NH_3*)) of 15 doped clusters (i.e., Ti_3Mn, Ti_3Fe, Ti_3Co, Ti_3Ni, Ti_3Cu, V_3Mn, V_3Fe, V_3Co, V_3Ni, V_3Cu, Cr_3Mn, Cr_3Fe, Cr_3Co, Cr_3Ni, and Cr_3Cu).[3]

Systems	ΔG(N_2*-NNH*) (eV)	ΔG(NH_2*-NH_3*) (eV)	ΔGmax(eV)
Cr_3Fe	0.24	0.21	0.24
Cr_3Co	0.37	0.13	0.37
Cr_3Ni	0.75	-0.49	0.75
Cr_3Cu	0.91	-0.26	0.91
Cr_3Mn	0.15	0.48	0.48
Ti_3Mn	-0.11	0.91	0.91
Ti_3Fe	0.18	0.44	0.44
Ti_3Co	0.45	0.42	0.45
Ti_3Ni	0.39	0.33	0.39
Ti_3Cu	0.58	0.31	0.58
V_3Mn	-0.07	0.57	0.57
V_3Fe	0.33	0.44	0.44
V_3Co	0.7	0.35	0.7
V_3Ni	0.75	0	0.75
V_3Cu	1.4	-0.11	1.4

Table **S11.** The calculated limiting potential (U_L) of M_3/V_O−$Mo_2TiC_2O_2$ SCCs and M_2M'/V_O−$Mo_2TiC_2O_2$ for efficient NRR[4]

Systems	U_L (V)
Ru_3/V_O−$Mo_2TiC_2O_2$	-0.32
Fe_3/V_O−$Mo_2TiC_2O_2$	-0.52
Rh_3/V_O−$Mo_2TiC_2O_2$	-0.23
Co_3/V_O−$Mo_2TiC_2O_2$	-0.44
Ni_3/V_O−$Mo_2TiC_2O_2$	-0.42
Fe_2Ru/V_O−$Mo_2TiC_2O_2$	-0.44
$FeRu_2/V_O$−$Mo_2TiC_2O_2$	-0.41

Table **S12.** The calculated formation energy (E_f) and electrochemical dissolution potentials (U_{diss}) of M@$Mo_2TiC_2O_2$ MXene, where the related data has also been provided.

Systems	E_{MXene}	E_{TM}	E_{Total}	E_f	U^0_{diss}	*ne*	U_{diss}
Ti@$Mo_2TiC_2O_2$	-597.56	-2.14	-604.96	-5.27	-1.63	2	1.00
V@$Mo_2TiC_2O_2$	-597.56	-3.55	-604.69	-3.58	-1.18	2	0.61
Cr@$Mo_2TiC_2O_2$	-597.56	-4.66	-604.20	-1.98	-0.91	2	0.08
Zr@$Mo_2TiC_2O_2$	-597.56	-2.35	-606.01	-6.10	-1.45	4	0.08
Nb@$Mo_2TiC_2O_2$	-597.56	-1.01	-605.81	-7.24	-1.10	3	1.31
Mo@$Mo_2TiC_2O_2$	-597.56	-4.65	-605.37	-3.16	-0.2	3	0.85
Hf@$Mo_2TiC_2O_2$	-597.56	-3.19	-606.61	-5.86	-1.55	4	-0.08
Ta@$Mo_2TiC_2O_2$	-597.56	-3.52	-606.70	-5.62	-0.6	3	1.27
W@$Mo_2TiC_2O_2$	-597.56	-4.57	-606.23	-4.11	0.1	3	1.47

Table **S13.** The calculated formation energy (E_f) and electrochemical dissolution potentials (U_{diss}) of M/$Mo_2TiC_2O_2$ MXene, where the related data has also been provided.

Systems	E_{MXene}	E_{TM}	E_{Total}	E_f	U^0_{diss}	*ne*	U_{diss}
Ti/$Mo_2TiC_2O_2$	-606.26	-2.14	-614.43	-6.03	-1.63	2	1.38
V/$Mo_2TiC_2O_2$	-606.26	-3.55	-613.58	-3.76	-1.18	2	0.70
Cr/$Mo_2TiC_2O_2$	-606.26	-4.66	-612.79	-1.86	-0.91	2	0.02
Zr/$Mo_2TiC_2O_2$	-606.26	-2.35	-615.54	-6.92	-1.45	4	0.28
Nb/$Mo_2TiC_2O_2$	-606.26	-1.01	-614.87	-7.59	-1.10	3	1.43
Mo/$Mo_2TiC_2O_2$	-606.26	-4.65	-613.02	-2.11	-0.2	3	0.50
Hf/$Mo_2TiC_2O_2$	-606.26	-3.19	-615.94	-6.49	-1.55	4	0.07
Ta/$Mo_2TiC_2O_2$	-606.26	-3.52	-616.34	-6.56	-0.6	3	1.59
W/$Mo_2TiC_2O_2$	-606.26	-4.57	-615.25	-4.42	0.1	3	1.57

REFERENCES

(1) Li, L.; Wang, X.; Guo, H.; Yao, G.; Yu, H.; Tian, Z.; Li, B.; Chen, L. Theoretical Screening of Single Transition Metal Atoms Embedded in MXene Defects as Superior Electrocatalyst of Nitrogen Reduction Reaction. *Small Methods* **2019**, *3* (11), 1900337. https://doi.org/10.1002/smtd.201900337.

(2) Cheng, Y.; Dai, J.; Song, Y.; Zhang, Y. Single Molybdenum Atom Anchored on 2D Ti_2 NO_2 MXene as a Promising Electrocatalyst for N_2 Fixation. *Nanoscale* **2019**, *11* (39), 18132–18141. https://doi.org/10.1039/C9NR05402B.

(3) Yu, R.; Liu, Z.; Legut, D.; Sun, J.; Zhang, Q.; Francisco, J. S.; Zhang, R. Highly Efficient and Selective Nitrogen Reduction Reaction Catalysis of Cluster-Modified

MXene Nanosheets. *ACS Catal.* **2024**, *14* (14), 10568–10582. https://doi.org/10.1021/acscatal.4c01369.

(4) Shu, P.; Qi, X.; Peng, Q.; Chen, Y.; Gong, X.; Zhang, Y.; Ouyang, F.; Sun, Z. Heterogeneous Metal Trimer Catalysts on Mo2TiC2O2 MXene for Highly Active N2 Conversion to NH3. *Molecular Catalysis* **2023**, *539*, 113036. https://doi.org/10.1016/j.mcat.2023.113036.